



Coin-structured tunable beam shaping assembly design for accelerator-based boron neutron capture therapy for tumors at different depths and sizes

Zhao-Peng Qiao^{1,2,4} · Yao-Cheng Hu^{1,2} · Quan-Xu Jiang^{1,2} · Jing-Jing Fan^{1,2} · Isao Murata⁴ · Rui-Rui Liu⁵ · Bo Wang⁶ · Sheng Wang^{1,2,3}

Received: 25 May 2023 / Revised: 8 August 2023 / Accepted: 22 August 2023 / Published online: 30 November 2023

© The Author(s), under exclusive licence to China Science Publishing & Media Ltd. (Science Press), Shanghai Institute of Applied Physics, the Chinese Academy of Sciences, Chinese Nuclear Society 2023

Abstract

In the past decade, boron neutron capture therapy utilizing an accelerator-based neutron source (ABNS) designed primarily for producing epithermal neutrons has been implemented in the treatment of brain tumors and other cancers. The specifications for designing an epithermal beam are primarily based on the IAEA-TECDOC-1223 report, issued in 2001 for reactor neutron sources. Based on this report, the latest perspectives and clinical requirements, we designed an ABNS capable of adjusting the average neutron beam energy. The design was based on a 2.8 MeV, 20 mA proton beam bombarding a lithium target to produce neutrons that were subsequently moderated and tuned through a tunable beam shaping assembly (BSA) which can modify the thicknesses and materials of the coin-shaped moderators, back reflectors, filters, and collimators. The simulation results demonstrated that epithermal neutron beams for deep seated tumor treatment, which were generated by utilizing magnesium fluoride with lengths ranging between 28 and 36 cm as the moderator, possessed a treatment depth of 5.6 cm although the neutron flux peak shifts from 4.5 to 1.0 keV. When utilizing a thinner moderator, a less accelerated beam power can meet the treatment requirements. However, higher powers reduced the treatment time. In contrast, employing a thick moderator can reduce the skin dose. In scenarios that required relatively low energy neutron beams, the removal of the thermal neutron filter can raise the thermal neutron flux at the beam port. And the depth of the dose rate peak could be adjusted between 0.25 and 2.20 cm by combining magnesium fluoride and polyethylene coins of different thicknesses. Hence, this device has a better adaptability for the treatment of superficial tumors. Overall, the tunable BSA provides greater flexibility for clinical treatment than common BSA designs that can only adjust the port size.

Keywords Boron neutron capture therapy (BNCT) · Accelerator-based neutron source (ABNS) · Beam shaping assembly (BSA) · Treatment depth

This study was supported by the National Nature Science Foundation of China (No. 1210050454) and the program of Chinese Scholarship Council (No. 202106280126).

✉ Sheng Wang
shengwang@xjtu.edu.cn

¹ Department of Nuclear Science and Technology, School of Energy and Power Engineering, Xi'an Jiao-Tong University, No. 28, Xianning West Road, Xi'an 710049, China

² XJTU-Huzhou Neutron Science Laboratory, Science Valley Medium-Sized Building #1, Huzhou 313000, China

³ RIKEN Center for Advanced Photonics, RIKEN, Wako, Saitama 351-0198, Japan

⁴ Division of Sustainable Energy and Environmental Engineering, Graduate School of Engineering, Osaka University, Suita, Osaka 565-0871, Japan

⁵ Department of Radiation Oncology and Winship Cancer Institute, Emory University, Atlanta, GA, USA

⁶ School of Mathematics and Statistics, NingBo University, No.818 Fenghua Road, Ningbo 315211, China

1 Introduction

Boron neutron capture therapy (BNCT) is a binary radiotherapy method used for treating a variety of cancers, at present, mainly including head and neck tumors, brain cancer melanoma and so on [1–6]. This technique involves the first administration the highly selective tumor-targeting agent containing ^{10}B to the patient, followed by irradiation with either epithermal or thermal neutrons depending on the tumor depth [7]. As the epithermal neutrons penetrate the tissue, they are moderated and subsequently captured by the ^{10}B atoms in the tumor cells. This leads to a nuclear reaction that produces high linear energy transfer (LET) α and ^7Li ions, which have a short range radiation and destroy the targeted cells while minimizing damage to the surrounding tissues [8–10].

Until the beginning of this century, the main method for conducting BNCT experiments was to use reactor-based neutron sources [11–13]. The first accelerator-based neutron source (ABNS) for BNCT in the world was a cyclotron-based neutron source (C-BENS) that manufactured and installed at Kyoto University in 2008 [14]. Subsequently, owing to the rapid development of the accelerator-based boron neutron capture therapy (AB-BNCT) in the last 10 years, it has received increasing attention worldwide. This is especially because in 2020, the same facility with C-BENS at the Kansai BNCT Medical Center in Japan was allowed by the Japanese Ministry of Health, Labor, and Welfare to accept patients for routine treatment in [15], the AB-BNCT has been paid more and more attention all over the world. Along with Japan, other countries, including China, South Korea, the US, the UK, Russia and so on, are investing in the design and manufacture of AB-BNCT facilities to primarily provide epithermal neutron beams for the treatment of deep-seated tumors.

The design requirements for epithermal beams are primarily based on the IAEA-TECDOC-1223 [7], a report issued in 2001 on reactor neutron sources. In this report, the region of the epithermal neutron, which is used for deep-seated tumors in BNCT, is recommended from 0.5 to 10 keV, based on the BNCT experience with neutron beams from reactors. However, there are also different opinions about the upper limit of epithermal neutron beam for AB-BNCT under the current situation of ABNS. The C-BENS was designed to generate epithermal neutrons with energies of 0.5 to 40 keV [14, 16]. Torres-Sánchez P., et al. [17] suggested that neutrons above 10 keV can be useful for BNCT and that the exact limit of the epithermal range should depend on the location of the tumor. Their other research indicated that the upper limit could be incremented up to 15 to 20 keV under accelerator-based neutron source (ABNS) conditions [18] and they discussed

the significant impact of different regions of the epithermal neutron on the beam shaping assembly (BSA) design [19]. Bisceglie E., et al. [20] suggested the fast neutrons ($E_n > 50$ keV) in the therapeutic beam should be minimized for their responsibility of a large surface dose, but neutrons with energy of slightly above 10 keV could shift the therapeutic gain toward higher. However, Hervé M., et al. [21] suggested the lower epithermal energy neutrons for AB-BNCT tumor irradiation could improve treatment efficacy by delivering more therapeutic dose while reducing the dose in healthy tissues. Seki R., et al. [22] against the extension of the upper limit of epithermal neutron for BNCT more than 10 keV because of protection of normal tissues from receiving an intolerable amount of dose.

In addition to treating deep tumors with epithermal neutrons, BNCT can also be expected to treat skin cancer, such as malignant melanoma and superficial tumors such as angiosarcoma and malignant meningioma, with thermal neutron. In addition, certain experiments on animal require neutron beams with lower average energy [23, 24]. To respond to these needs, for the reactor-based neutron source, both epithermal and thermal neutron beams could be induced easily at the same time, such as at the Kyoto University Research Reactor (KUR) [25], the In-hospital neutron irradiator (IHNI) [26], etc. For the AB-BNCT facilities, most of the current BSA designs are working on epithermal neutron beams [16, 27–34]. In order to adapt the epithermal neutron beam to superficial tumor treatment, several measures have been adopted found and found to be effective. Herrera M.S., et al. [35] purposed to wear a bolus to thermalize the neutron beam. Hu N., et al. [36, 37] made some modifications, such as put a polyethylene (PE) plate at the beam port to shift the dose peak to the skin.

We designed an AB-BNCT facility based on the $\text{Li}(p,n)$ reaction, which was manufactured and installed at the XJTU-Huzhou Neutron Science Laboratory. The facility uses a radio frequency quadrupole field accelerator with a 2.8 MeV, 20 mA proton beam to bombard a fixed lithium target which is cooled by water. To reduce the cooling pressure, the proton beam spot homogenization, microchannel structure design and flow rate increase were measured. The generated neutrons are moderated by a beam shaping assembly to obtain a neutron beam for tumor treatment. To address the aforementioned challenges, we designed a BSA with adjustable moderator both for thickness and material, which accompanied by lead rings of different thicknesses, filters of different materials, and collimators of varying diameters. These components are named as moderator, back reflector, filter and collimator coins, not only because their physical resemblance to coins, but also because they can achieve greater denominations through combination. In this case, the adjustability of the BSA is achieved through the combination of these coin-shaped components of different parameters,

hence, this design is referred to as the Coin-structured Tunable Beam Shaping Assembly. This ABNS with a tunable BSA can easily obtain epithermal neutron beams with different upper limits and neutron beams of relatively low energy.

2 Materials and methods

2.1 BSA design

In this work, we specify that the set direction is along the proton beam direction. Figure 1 shows a cross section view of the target system and side view of some backup coins.

The target, which contained a lithium layer and copper substrate with cooling water, is connected to a section of bellows which allowed the target to move back and forth in the direction of the proton beam. Based on the conclusions obtained from a previous work [38], a lithium layer with a thickness of 150 μm was used and the corresponding neutron yield was 1.40×10^{12} n/mC under the condition of 2.8 MeV incident protons. The neutron spectrum was recorded and set as the initial source term for subsequent neutron transportation in the BSA to reduce the calculation time.

Along the beam, a cylindrical moderator made of magnesium fluoride was placed behind the target. As discussed in previous studies [19, 39–41], Magnesium fluoride is the preferred moderator material for our proton beam and target scheme. We designed the moderator as six coins, each with a diameter of 50 cm and thicknesses of 2 cm for one coin, 4 cm for four coins, and 20 cm for one coin. Unlike

dividing the moderator into two or more layers with fixed thicknesses and installing them as the moderator [16, 27, 42–44], designing the moderator as multiple coins with different thicknesses facilitates flexible combinations to adjust the neutron energy spectrum. In this work, the density of magnesium fluoride is 2.8 g/cm^3 unless otherwise specified. Taking into account several factors such as the density influence on neutronic properties [38], processing difficulty, cost and potential density inhomogeneity, a density of 2.8 g/cm^3 is a conservative but reasonable assumption, although higher-density magnesium fluoride blocks may be processed.

There are three kinds of reflectors are to reflect neutrons back to the moderator to reduce neutron leakage and increase the neutron flux at the port. First, the moderator was encased in lead of a thickness of 15 cm as the side reflector, and the length of this lead cylinder that also named moderating tunnel is 40 cm. A hollow cylindrical back reflector was arranged in front of tunnel to wrap the bellows as the back reflector. During operation, the position of the port remained unchanged. To ensure the largest possible neutron flux at the port, after embedding the appropriate moderator coins in the tunnel and pressing them tightly to cling to the filter, the target was moved close to the moderator by telescoping the bellows. Then space in the tunnel was filled with backup lead rings, also known as back reflector coins.

Behind the moderator were thermal neutron and gamma-ray filters used to reduce doses harmful to patients. The thickness and material of these filters can also be changed by backup filter coins according to requirements. We calculated and compared the effect and influence of LiF, Cd, Bi, and

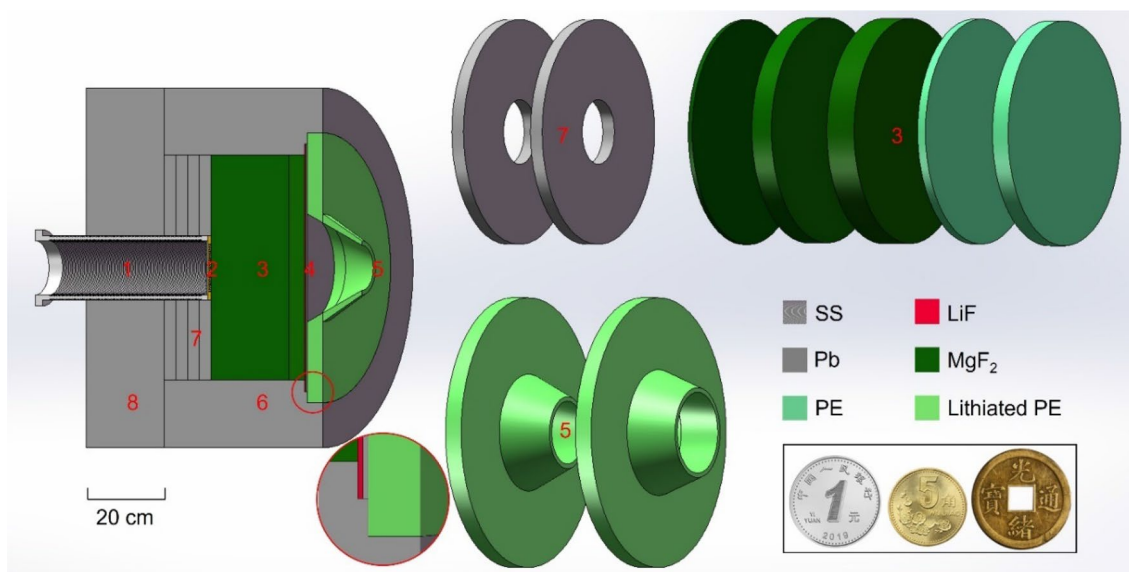


Fig. 1 (Color online) Cross section of the Coin-structured beam shaping assembly and side view of some backup coins. 1: bellows, 2: lithium target, 3: moderator coins, 4: thermal neutron filter and gamma-

ray filter coins, 5: collimator coins and beam port, 6: side reflector, 7: back reflector coins, 8: back reflector. The black wireframe in the corner shows modern and ancient Chinese coins

Pb as filters and selected materials according to the actual situation of the equipment.

Next the collimator was made of PE mixed with natural LiF at a 60% mass fraction. A series of collimators with apertures ranging from 10 to 20 cm, called collimator coins, were designed to meet different needs. In order to mitigate the detrimental effects of neutron leakage, a two-stage step design was employed which incorporated a filter and collimator whose diameters were 55 cm and 60 cm respectively (enlarged part of Fig. 1).

Table 1 The dominant radionuclides generated by cadmium filter after 2 h of operation

No	Nuclides	Activity (Bq/cc)	Photon dose (μSv/h)	Half-life (s)
1	^{111m} Cd	1.8717 × 10 ⁷	6.6180 × 10 ³	2.912 × 10 ³
2	¹¹⁵ Cd	9.2655 × 10 ⁶	2.2467 × 10 ³	1.925 × 10 ⁵
3	¹¹⁷ Cd	9.1262 × 10 ⁶	1.1017 × 10 ⁴	8.960 × 10 ³
4	¹⁰⁷ Cd	4.3570 × 10 ⁶	1.2059 × 10 ¹	2.340 × 10 ⁴
5	^{107m} Ag	4.3196 × 10 ⁶	2.5452 × 10 ¹	4.430 × 10 ¹
6	^{117m} In	2.5845 × 10 ⁶	2.8523 × 10 ²	6.972 × 10 ³
7	¹¹⁷ In	1.6781 × 10 ⁶	1.4631 × 10 ³	2.592 × 10 ³
8	^{115m} In	1.3002 × 10 ⁶	2.5861 × 10 ²	1.615 × 10 ⁴
9	^{117m} Cd	1.1463 × 10 ⁶	2.4533 × 10 ³	1.210 × 10 ⁴
10	^{115m} Cd	5.9512 × 10 ⁴	2.2342 × 10 ⁰	3.850 × 10 ⁶

Since our design requires disassembly and replacement of the moderator coins, especially during the commissioning phase of the equipment, the neutron induced radioactivity of different candidate materials for each component mentioned above was considered while selecting the appropriate materials. This was to reduce the risk of exposure to irradiation that may occur during the change process (Table 1).

2.2 Epithermal neutron beam

The five recommended parameters for epithermal neutron beams are given in IAEA-TECDOC-1223 [7], and the details are listed in Table 2. Considering the discussions of different upper limit of the epithermal neutron, we performed comparative calculations for 0.5 to 10 keV and 0.5 to 40 keV, as listed in Table 2. Considering that the energy of the generated neutrons from the Li(p,n) reaction with a 2.8 MeV proton is within 1.1 MeV, the fast neutron contamination calculation we refer to the literature [40] and it is defined by

$$D_f / \Phi_{epi} = \int_{epiTHR.}^{1.1MeV} \Phi(E) \cdot K(E) dE / \int_{0.5eV}^{epiTHR.} \Phi(E) dE \quad (1)$$

Here, Φ and K denote the neutron flux at the port and the ICRU-63 [45] neutron kerma coefficient [Gy cm²] for soft tissue. In such a case, the contamination should be less than

Table 2 Epithermal neutron beam parameters under Magnesium fluoride with different thicknesses

Magnesium fluoride thickness (cm)	Epith. limits	Φ_{epi} (n/cm ² s)	Φ_{th} / Φ_{epi}	D_{fast} / Φ_{epi} (Gy cm ²)	D_f / Φ_{epi} (Gy cm ²)	J_n / Φ_n	Min beam power (kW)
20	0.5 eV–10 keV	2.77 × 10 ⁹	0.0298	1.90 × 10 ⁻¹²	9.68 × 10 ⁻¹⁴	0.694	21.0
	0.5 eV–40 keV	3.55 × 10 ⁹	0.0232	1.05 × 10 ⁻¹²	7.53 × 10 ⁻¹⁴		16.3
22	0.5 eV–10 keV	2.52 × 10 ⁹	0.0310	1.40 × 10 ⁻¹²	9.38 × 10 ⁻¹⁴	0.694	23.0
	0.5 eV–40 keV	3.13 × 10 ⁹	0.0250	7.60 × 10 ⁻¹³	7.55 × 10 ⁻¹⁴		18.5
24	0.5 eV–10 keV	2.28 × 10 ⁹	0.0324	1.05 × 10 ⁻¹²	9.21 × 10 ⁻¹⁴	0.695	25.5
	0.5 eV–40 keV	2.74 × 10 ⁹	0.0270	5.55 × 10 ⁻¹³	7.65 × 10 ⁻¹⁴		21.2
26	0.5 eV–10 keV	2.05 × 10 ⁹	0.0347	7.86 × 10 ⁻¹³	9.13 × 10 ⁻¹⁴	0.696	28.3
	0.5 eV–40 keV	2.40 × 10 ⁹	0.0296	4.03 × 10 ⁻¹³	7.80 × 10 ⁻¹⁴		24.2
28	0.5 eV–10 keV	1.83 × 10 ⁹	0.0368	5.94 × 10 ⁻¹³	9.30 × 10 ⁻¹⁴	0.698	31.7
	0.5 eV–40 keV	2.09 × 10 ⁹	0.0323	2.95 × 10 ⁻¹³	8.14 × 10 ⁻¹⁴		27.8
30	0.5 eV–10 keV	1.62 × 10 ⁹	0.0400	4.51 × 10 ⁻¹³	9.65 × 10 ⁻¹⁴	0.699	35.8
	0.5 eV–40 keV	1.81 × 10 ⁹	0.0358	2.16 × 10 ⁻¹³	8.64 × 10 ⁻¹⁴		32.0
32	0.5 eV–10 keV	1.44 × 10 ⁹	0.0436	3.46 × 10 ⁻¹³	1.01 × 10 ⁻¹³	0.701	40.4
	0.5 eV–40 keV	1.57 × 10 ⁹	0.0397	1.60 × 10 ⁻¹³	9.25 × 10 ⁻¹⁴		36.8
34	0.5 eV–10 keV	1.27 × 10 ⁹	0.0475	2.64 × 10 ⁻¹³	1.08 × 10 ⁻¹³	0.702	45.8
	0.5 eV–40 keV	1.37 × 10 ⁹	0.0440	1.17 × 10 ⁻¹³	1.00 × 10 ⁻¹³		42.4
36	0.5 eV–10 keV	1.11 × 10 ⁹	0.0521	2.04 × 10 ⁻¹³	1.15 × 10 ⁻¹³	0.704	52.1
	0.5 eV–40 keV	1.19 × 10 ⁹	0.0489	8.58 × 10 ⁻¹⁴	1.08 × 10 ⁻¹³		48.9
IAEA recommendation	0.5 eV–10 keV	> 1 × 10 ⁹	< 0.05	< 2 × 10 ⁻¹³	< 2 × 10 ⁻¹³	> 0.70	–

1.0×10^{-12} Gy cm^2 . Similarly, gamma-ray contamination is gamma-ray heat divided by the epithermal neutron flux.

A 20 cm cubic block filled with soft tissue (ICRU four component) was used a phantom to evaluate the absorbed dose and therapeutic potential of the different neutron beams. The concentration of ^{10}B in normal tissues and tumors was set as 18 and 65 ppm, respectively. The relative biological effectiveness (RBE) of nitrogen, hydrogen, and gamma-rays were assumed to be 3.2, 3.2, and 1.0, respectively. The compound biological effectiveness (CBE) for tumor and normal tissues was assumed to be 3.8 and 1.35, respectively. The total dose was calculated using Eq. (2) as follows:

$$D = CBE_B D_B + RBE_N D_N + RBE_H D_H + RBE_\gamma D_\gamma \quad (2)$$

where D_B , D_N , D_H , D_γ are the four absorbed doses in BNCT, namely the boron, thermal, fast neutron and gamma-ray doses, respectively.

The irradiation time, also called the treatment time (TT), was determined by setting the point dose limit on the normal tissue to 12.5 Gy [15]. According to that the sufficient dose for killing a tumor is at least 30 Gy, the maximum depth in the tumor that can be reached by 30 Gy within the irradiation time is the treatment depth (TD) [14]. And the depth where could reach 15 Gy within the irradiation time means that treatment can be completed with two irradiations from different directions. Section 3.2 discusses the detailed effects of parameters such as moderator thickness and density, the ratio of boron concentration in tumor and normal tissue (T/N) and beam power of accelerator on the dose rate and TD.

2.3 Relatively low energy neutron beam

In order to adapt the epithermal neutron beam to superficial tumor treatment, we can place the thermal neutron moderator inside the BSA, that is, use a combination of a more efficient material and magnesium fluoride as the moderator. This is in addition to the measures that could be adopted, such as a bolus adhering to the skin and dose distribution shifter at the port. We compared heavy water, BeO , and PE. We chose PE as a further moderator after calculations and comparisons, and considering cost and other factors. Multiple PE disks, each with a thickness of 2 cm and diameter identical to that of the magnesium fluoride disks, served as moderator coins for the tunable BSA alongside the MgF_2 disks. The effects of the PE placement and thickness on the outgoing neutron beam are discussed. Compared to its non-disassemblable counterparts, this tunable BSA facilitates the utilization of both epithermal and thermal neutron moderators, as well as the removal of the thermal neutron filter at the port in favor of a thicker gamma filter, leading to a higher thermal neutron flux. To evaluate the treatment

effect of relatively low energy neutron beams, the RBE, TT, and TD doses were also calculated.

2.4 Multi-size apertures

The moderator can be adjusted, to adapt it for treating tumors at different depths. By adjusting the diameter of the port, the treatment requirements for tumors of different sizes can be met. Although an adjustable aperture design is common in BSA, we mainly focus on the points directly related to this coin-structured tunable BSA design, such as the impact of using the same collimator port on the neutron beam after changing the moderator and adaptation of the moderator after selecting the port with a certain diameter.

3 Results and discussions

3.1 Residual radioactivity induced in the BSA

Taking the scenario of shutting down after running at full accelerated beam power of 56 kW for 2 h as an example, the photon dose rate at the treatment position due to the residual radioactivity induced in each component of BSA is shown in Fig. 2. It can be seen that the neutron-induced radioactivity of cadmium is the highest among the alternative materials for each component. After 2 h of irradiation, the information of dominant radioisotopes generated by the Cd filter, such as ^{115}Cd , ^{117}Cd , and $^{117\text{m}}\text{In}$, are listed in Table 1. The entire Cd filter that with a thickness of 0.2 cm has a radioactivity level of up to 3.7×10^{10} Bq, with a gamma dose rate of 2.4×10^4 $\mu\text{Sv/h}$ at the treatment position at end of irradiation. Replacing the Cd coin with 0.3 mm LiF coin can significantly

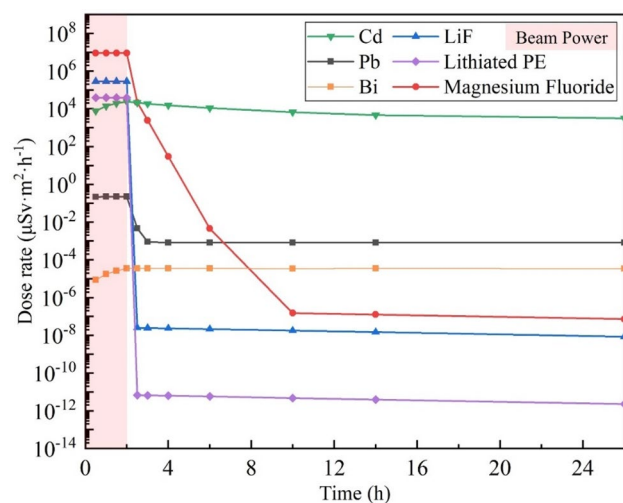


Fig. 2 (Color online) The photon dose rate of the BSA components at the treatment position due to the neutron induced radioactivity

reduce the induced radioactivity to negligible level without affecting the parameters of the outgoing neutron beam, especially the ratio between thermal and epithermal neutrons. With the exception of Cd, the induced radioactivity of other components within the acceptance after cooling for 4 h. However, it should be noted that LiF generates ^3H with a half-life of 12.4 years after neutron irradiation, requiring proper handling of thermal neutron filters made of lithium fluoride and collimators containing lithium fluoride after decommissioning. But condensing that tritium could be also produced in the target by the $^6\text{Li}(n, t)^4\text{He}$ reaction, the management of the tritium is necessary for such a facility [46]. Bi generates ^{210}Bi after neutron irradiation, which has a half-life of approximately 5 days. Pb and Magnesium fluoride primarily generate ^{209}Pb and ^{24}Na , respectively, both of which have a half-life of less than 1 day. As for the gamma filter, lead and bismuth exhibit little difference in neutron performance and activation, but lead is easier to obtain. Therefore, we used LiF and Pb for the thermal neutron and gamma filters, respectively.

3.2 Epithermal neutron beam parameters

The results of the neutron beam using magnesium fluoride as a moderator with a density of 2.8 g/cm^3 and a beam port with a diameter of 10 cm and different thicknesses are shown in Table 2. We compared the results obtained using 10 and 40 keV as the upper limit of the epithermal energy. For all the cases, the epithermal neutron flux is greater than $1 \times 10^9\text{ cm}^{-2}\text{ s}^{-1}$ under full beam power of 56 kW. When the thickness of the Magnesium fluoride moderator is less than 24 cm, an upper limit of 40 keV increases the epithermal neutron flux by 20% or more compared with that obtained 10 keV. When the thickness of the magnesium fluoride moderator is between 24 and 32 cm, the rate of increase is between 20 and 10%. When the thickness of the magnesium fluoride moderator is greater than 32 cm, this increase rate is less than 10%. This is because a thicker moderator moderated neutrons more completely, resulting in fewer neutrons with energies between 10 and 40 keV. During operation, when a thinner moderator (less than 32 cm) is used, the different upper limits of the epithermal energy have a significant impact on the epithermal neutron flux. This, in turn, obviously affects the treatment time, and hence needs to be carefully considered. The minimum accelerated beam power required refers to the power at which the epithermal neutron flux reaches $1 \times 10^9\text{ cm}^{-2}\text{ s}^{-1}$. When the upper limit of the epithermal neutrons increases or the thickness of the moderator decreases, the minimum required beam power correspondingly decreases. The spectrums corresponding to partially different thicknesses of magnesium fluoride, ranging from 20 to 36 cm, are shown in Fig. 3. Their respective peak energy values are 16, 9.2, 4.5, 2.3, and 1.0 keV. This

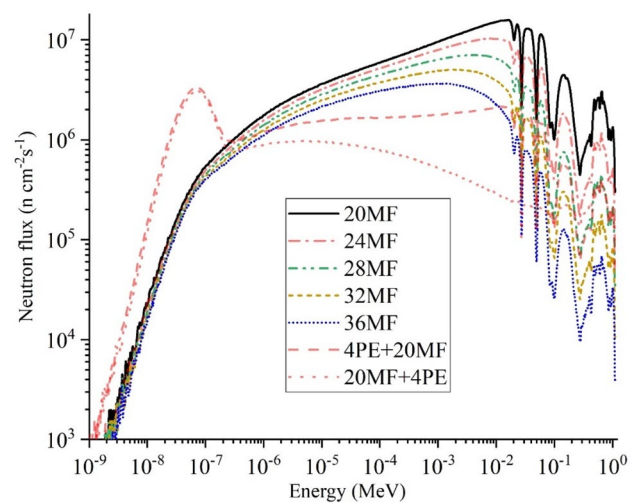


Fig. 3 (Color online) Neutron spectra corresponding to different thicknesses of Magnesium fluoride or Magnesium fluoride with PE ranging from 20 to 36 cm

indicates that the average energy of the epithermal neutron beam can be conveniently regulated by adjusting the moderator coins.

For the forward beam direction, the ratio of the neutron current to the flux (c/f , J_n/Φ_n) increases with the thickness of the moderator, which indicates an increase in the fraction of neutrons moving in the forward beam direction. Table 2 shows that when magnesium fluoride with a thickness range of 26–36 cm is used as a moderator, the c/f range is 0.7000 ± 0.004 , which meets the requirements. The gamma contamination and ratio of the thermal neutron flux to the epithermal neutron flux always meets the requirements within the calculation range and are not discussed further.

Adopting different divisions of the epithermal range not only has an intuitive impact on the epithermal neutron flux but also affects the fast neutron contamination that defined in Eq. (1). In comparison, a broader epithermal range results in a fast neutron contamination level that is approximately 50% of that observed with a narrower range. As per the guidelines set forth by the International Atomic Energy Agency (IAEA), the fast neutron contamination exerts a direct influence on the minimum thickness of the moderator required. However, in this design, apart from considering the beam parameters, we determined the optimal thickness of the moderator through the TD that discussed below.

The dose rate distributions along the depth and total dose of the neutron beams at different thicknesses of the moderator in a soft tissue phantom are presented in Fig. 4a and Table 3. At each corresponding neutron beam and the treatment time of different moderator thickness, the accumulated dose distribution in the tumor varies with the depth, as shown in Fig. 4b. When the thickness of the moderator is relatively thin (e.g., 20 cm), the treatment depth is shallow

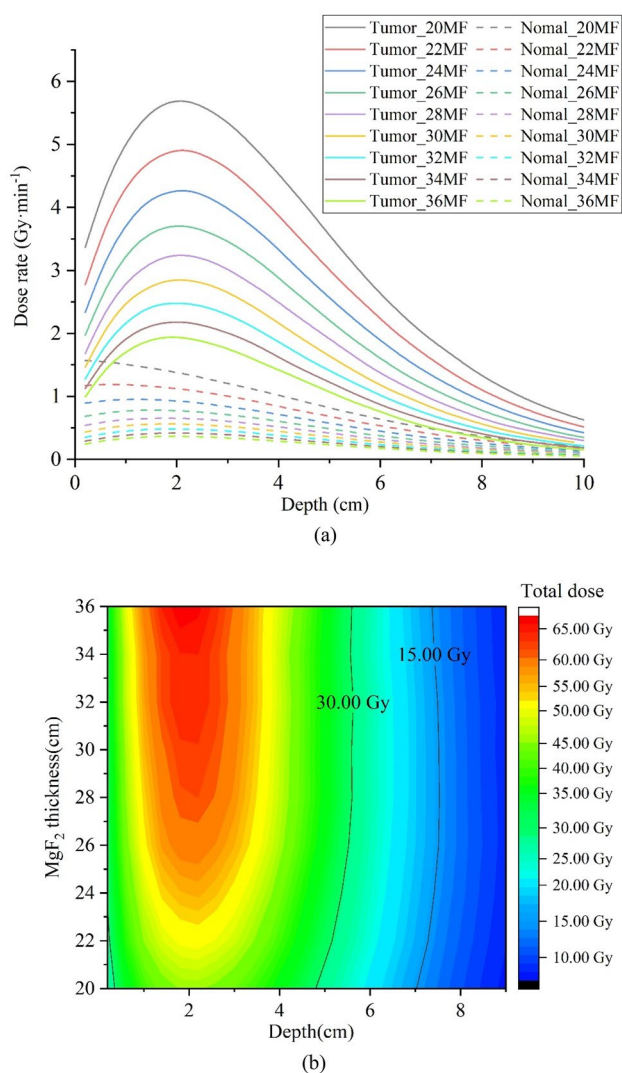


Fig. 4 (Color online) Therapy parameters of neutron beams at different thicknesses of the moderator in a soft tissue phantom: **a** dose rate distributions along the depth; **b** total dose distributions along the depth

(approximately 4.8 cm). Within the scope of this discussion, as the thickness of the moderator increases, the treatment depth gradually increases until it reaches a constant depth of 5.6 cm when the thickness is greater than 28 cm. This is because when the moderator is thin, the fast neutron flux is high, and the fast neutron dose is relatively high among the four doses of BNCT, limiting the treatment depth. Table 3 presents the fast neutron dose converted to photon equivalent, the total dose on the skin, and their respective ratio. As the thickness of the moderator increases from 20 to 36 cm, the proportion of the fast neutron dose decreases gradually from 71 to 28%, and the total dose at the skin surface decreases distinctly at each corresponding treatment time. For example, when the thickness of the moderator is increased from 28 to 36 cm, the dose at the skin surface is

reduced by 18% from 10.29 to 8.39 Gy. This is consistent with the findings of Seki R., et al. (2017) [22].

The results presented in Fig. 4 also demonstrate that the 15 Gy isodose curve attains its maximum value of approximately 7.6 cm at a moderator thickness of 28 cm. It is worth noting that in Ref. [14], the C-BENS treatment beam delivers 30 and 15 Gy at depths of 5.5 and 8 cm, respectively, when the T/N was approximately 3.5. Although the spectrum of the epithermal neutron beam designed in this study differ from that of C-BENS, it achieved a similar TD. Nonetheless, if the boron concentrations in the tumor and normal tissue is assumed to be 65 and 6.5 ppm, respectively, and the CBE remains constant, the TD obtained for the magnesium fluoride moderator with a thickness of 28 cm can be increased to 6.4 cm. Moreover, a change in T/N can affect CBE [47], implying that the actual treatment depth can be augmented further. Hence, compared with fine-tuning the neutron spectrum of Li(p,n) by adjusting the moderator, enhancing the T/N ratio is indisputably more crucial.

According to a previous study [38], increasing the density of magnesium fluoride from 2.8 to 3.15 g/cm³ requires a reduction of approximately 3 cm in the moderator thickness to maintain the same level of fast neutron contamination. However, as described previously, the effect on the TD can be ignored within the thickness range of 28–36 cm of magnesium fluoride. This implies that the same therapeutic effect can be achieved by either increasing the density of magnesium fluoride to 3.15 g/cm³ or increasing the thickness of magnesium fluoride with a density of 2.8 g/cm³ by 3 cm. In both cases, the resultant therapeutic effect of the neutron beam remained unchanged. For instance, using magnesium fluoride with a thickness of 26 cm as the moderator, an increase in density from 2.8 to 3.15 g/cm³ increases the treatment depth from 5.5 to 5.6 cm, reducing the maximum dose to the skin by 12% (1.3 Gy) during the corresponding treatment time. This effect is almost equivalent to adding 3 cm of magnesium fluoride with a density of 2.8 g/cm³ to the moderator thickness to increase it from 26 to 29 cm, as shown in Table 2. Based on previous work, it can be concluded that using magnesium fluoride with a density of 2.8 g/cm³ as the moderator is sufficient and meets the requirements for the application. Increasing the density to 3.15 g/cm³ would result in significant manufacturing difficulties and costs without providing any notable advantages on the treatment depth.

At last, utilizing a thin moderator allows the accelerator to operate at a lower beam power to attain the required epithermal neutron flux. Since there is a proportional reduction in neutrons in each energy region after lowering the power, the shape of neutron spectrum remains unaltered, and the treatment parameters remains constant except for an inverse change in treatment time. Table 3 validates the effect of the accelerator operating at full accelerated beam power and

Table 3 Therapy parameters of neutron beams at different thicknesses of Magnesium fluoride and other factors

Magnesium fluoride thickness (m)	Max dose rate in norm. tiss. (Gy/min)	Treatment time (min)	Treatment depth (cm)	A: dose rate at skin (Gy/min)	Total dose at skin (Gy)	B: fast neutron dose rate at skin (Gy/min)	B:A
20	1.57	7.97	4.8	1.57	12.50	1.11	0.71
22	1.20	10.42	5.2	1.17	12.20	0.77	0.66
24	0.96	13.02	5.4	0.89	11.63	0.54	0.60
26	0.78	16.00	5.5	0.69	10.98	0.37	0.54
28	0.66	19.04	5.6	0.54	10.29	0.26	0.48
30	0.57	22.08	5.6	0.44	9.62	0.18	0.42
32	0.48	25.86	5.6	0.35	9.09	0.13	0.37
34	0.42	29.50	5.6	0.29	8.56	0.09	0.31
36	0.36	34.29	5.6	0.24	8.39	0.07	0.28
26, HD ¹	0.69	18.23	5.6	0.53	9.68	0.23	0.53
26, HT/N ²	0.59	21.12	6.4	0.59	12.45	0.37	0.59
26, LP ³	0.39	32.00	5.5	0.34	10.99	0.18	0.53

¹In this case, magnesium fluoride with a thickness of 28 cm and density of 3.14 g/cm³ was used. Magnesium fluoride with a density of 2.8 g/cm³ was used in all the other cases

²In this case, the boron concentrations in normal tissue and tumor are 6.5 ppm and 65 ppm respectively. In other cases, these two values are 18 ppm and 65 ppm, respectively

³In this case, the accelerated beam power was 29 kW. In other cases, the beam power is 56 kW

reduced power with a 26 cm magnesium fluoride moderator on dosimetric parameters.

In summary, adjusting the moderator thickness within a certain range will not influence the treatment depth, but increasing the thickness can significantly decrease the dose at the skin surface. Achieving an increase in the treatment depth by using a magnesium fluoride moderator with the highest density can be done by increasing the thickness of the moderator. Furthermore, under the condition where all other factors remain unchanged, the beam power change does not affect the treatment depth. Based on the analysis presented above, along with the literatures [7, 17–22, 39] discussing the upper limit of the epithermal energy range, we contend that neutrons of several keV offer greater treatment depth and reduced harmful dose to shallow normal tissue. Nevertheless, the elimination of high-energy neutrons inevitably results in a reduction of the neutron flux at the optimal energy level, consequently leading to longer treatment times and potential issues such as position misalignment. Given the current status of neutron source and boron drug development, employing epithermal neutrons slightly above 10 keV becomes unavoidable and necessary.

3.3 Relatively low energy neutron beam parameters

An example of 24 cm moderator thickness is shown by the three red curves in Fig. 3. When the moderators consisted of 24 cm of magnesium fluoride (a), 4 cm of PE with 20 cm of magnesium fluoride (b), and 20 cm of magnesium fluoride with 4 cm of PE (c), the proportion of high-energy neutrons

was progressively lower. Calculations demonstrated that under the three conditions (a), (b), and (c), the proportions of thermal neutrons to the total neutron flux were 2.46, 24.15, and 40.50%, respectively. The results indicate that replacing some of the magnesium fluoride with PE coins when using moderators of the same thickness can reduce the average energy of the original epithermal neutron beam. Additionally, placing PE behind magnesium fluoride has a more significant effect on energy reduction. This is due to the fact that the ¹H(n,elastic) cross-section of epithermal neutrons is larger compared to that of fast neutrons⁴⁸. Furthermore, the *c/f* of the neutron beam under these three conditions are 0.695, 0.734, and 0.760, respectively, indicating that the introduction of the PE plate can increase *c/f*. Consequently, the collimators and exit ports designed for epithermal neutron beams continue to satisfy the requirement.

Furthermore, the dose rate distribution of the outing neutron beam in the soft tissue phantom with depth was studied and the results showed in Fig. 5. When 22 cm of magnesium fluoride is used as the moderator, and the thermal neutron filter is removed and replaced with the same thickness of lead, the position of the dose rate peak moves from a depth of 2.20 to 1.95 cm, and the peak value increases by 6%. Both of those change benefits the treatment of shallow tumors. When the moderator is changed to a 20 cm magnesium fluoride coin and a 2 cm PE coin, the dose rate peak moves further to a depth of 0.85 cm. Increasing the thickness of PE to 4 and 6 cm moves the positions of the dose rate curve peaks to depths of 0.35 and 0.25 cm, respectively, while maintaining a constant thickness of magnesium fluoride constant as 20 cm. Calculations indicate that increasing the thickness

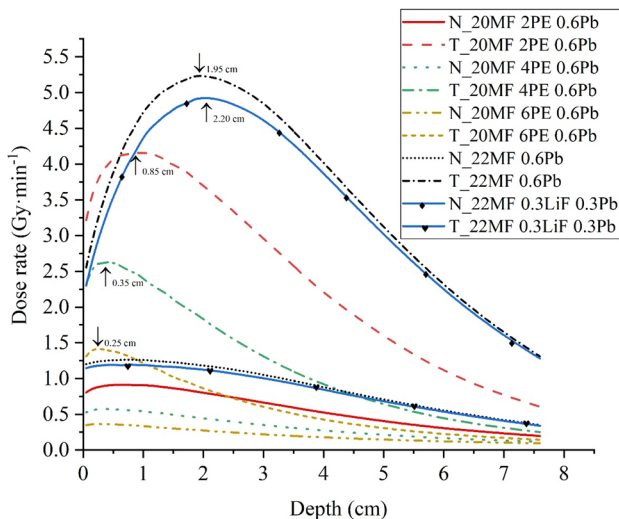


Fig. 5 (Color online) The dose rate distribution of the outing neutron beam of the different moderators and filters in the soft tissue phantom along the depth

of PE within 6 cm can accomplish tumor treatment within the dose tolerable by normal tissues (12.5 Gy), although the peak values of the thermal neutron flux and dose rate are reduced.

In summary, the use of magnesium fluoride and PE coins as moderators can further moderate the epithermal neutron beam and adjust the depth of the dose rate peak by changing the thickness of the PE. This method can ensure that the peak falls at the target irradiation depth while reducing the dose received by surrounding tissues under the premise of killing shallow tumors. Compared with the method of placing the PE plate at the port to change the depth of the dose peak, this design can also reduce the gamma dose caused by $H(n,\gamma)$ to some extent.

3.4 Multi-size apertures influence on beams

Table 2 illustrates that minor adjustments in the thickness of magnesium fluoride within a specific range have negligible effects on c/f , as exemplified by the 10 cm aperture. Therefore, although the moderator thickness is fine-tuned, the size of the collimator or the cone angle of the port need not be modified. Several collimators with aperture sizes between 10 and 20 cm were designed to conform to the parameters recommended by the International Atomic Energy Agency. The use of both magnesium fluoride and PE coins as moderators enhanced the c/f of the outgoing neutron beam compared to the use of magnesium fluoride alone, as mentioned in Sect. 3.4. Thus, the collimators initially designed for epithermal beams continue to remain functional. In addition, Ref. [17] suggests that the optimal neutron energy for treating deep-seated tumors partly depends on the size of the

beam aperture. In contrast to other BNCT facilities, which can only adjust the aperture size, the tunable BSA enables modulation of the neutron energy spectrum by varying the thickness of the moderator after determining the beam aperture size that achieves the optimal therapeutic outcome.

4 Conclusion

We designed a tunable BSA with adjustable thickness and moderator materials, which can adapt to different usage scenarios, including the generation of epithermal neutron beams and relatively low energy neutron beams, and operation under different accelerated beam powers. The adjustability of the device was achieved by combining coin-shaped components of different parameters; hence, this design is referred to as a coin-structured tunable beam-shaping assembly.

In the design of epithermal neutron beams, the TD remained constant at 5.6 cm when magnesium fluoride with a length of 28–36 cm was used as a moderator. Thinner moderators satisfied treatment requirements with a lower beam power, which partly reduces the cooling pressure on the lithium target and mitigates the need for stable accelerator operation. High-power operation provided a large flux of epithermal neutrons, which significantly reduced the TT. However, using thicker moderators also possesses certain advantages. For example, under the same treatment effect, the dose received by the skin decreased with increasing moderator thickness. Finally, high-density moderators require good density uniformity, which makes manufacturing difficult and expensive; however, this hardly increases the TD.

During the treatment of superficial tumors or while performing experiments such as the boron drug test, the thermal neutron flux at the skin can be increased by removing the thermal neutron filter. The depth at which the peak of the dose rate curve occurs can be adjusted within the range of 0.25–2.20 cm to meet different needs by combining magnesium fluoride and PE coins of different thicknesses.

All of these factors could provide greater flexibility for clinical treatment. However, some specific details of the actual processing of the BSA have not been considered. For example, because this design requires the frequent replacement of coins to improve equipment stability and prolong service life, each coin may need to be sealed in an aluminum shell, which will have a certain impact on the produced neutron beam.

Author contributions All authors contributed to the study conception and design. Material preparation, data collection and analysis were performed by Zhao-Peng Qiao, Yao-Cheng Hu, Quan-Xu Jiang, Jing-Jing Fan, Isao Murata, Rui-Rui Liu, Bo Wang, Sheng Wang. The first draft of the manuscript was written by Zhao-Peng Qiao and all authors

commented on previous versions of the manuscript. All authors read and approved the final manuscript.

Data availability The data that support the findings of this study are openly available in Science Data Bank at <https://www.doi.org/10.57760/sciencedb.j00186.00280> and <https://cstr.cn/31253.11.sciencedb.j00186.00280>.

Declarations

Conflict of interest The authors declare that they have no competing interests.

References

- S. Kawabata, M. Suzuki, K. Hirose et al., Accelerator-based BNCT for patients with recurrent glioblastoma: a multicenter phase II study. *Neuro Oncol. Adv.* **3**(1), vdab067 (2021). <https://doi.org/10.1093/oaajnl/vdab067>
- K. Hirose, A. Konno, J. Hiratsuka et al., Boron neutron capture therapy using cyclotron-based epithermal neutron source and borofalan (^{10}B) for recurrent or locally advanced head and neck cancer (JHN002): an open-label phase II trial. *Radiother. Oncol.* **155**, 182–187 (2021). <https://doi.org/10.1016/j.radonc.2020.11.001>
- J. Hiratsuka, N. Kamitani, R. Tanaka et al., Boron neutron capture therapy for vulvar melanoma and genital extramammary Paget's disease with curative responses. *Cancer Commun.* **38**(1), 38 (2018). <https://doi.org/10.1186/s40880-018-0297-9>
- C. Ceballos, J. Esposito, The BSA modeling for the accelerator-based BNCT facility at INFN LNL for treating shallow skin melanoma. *Appl. Radiat. Isot.* **67**, 274–277 (2009). <https://doi.org/10.1016/j.apradiso.2009.03.074>
- Z. Zhang, T. Liu, A review of the development of In-Hospital Neutron Irradiator-1 and boron neutron capture therapy clinical research on malignant melanoma. *Ther. Radiol. Oncol.* **2**, 49 (2018). <https://doi.org/10.21037/tro.2018.10.03>
- T.D. Malouff, D.S. Seneviratne, D.K. Ebner et al., Boron neutron capture therapy: a review of clinical applications. *Front. Oncol.* **11**, 601820 (2021). <https://doi.org/10.3389/fonc.2021.601820>
- IAEA-TECDOC-1223. Current status of neutron capture therapy. IAEA, **8**, 75–77 (2001). <https://doi.org/10.1111/j.1558-5646.2008.00544.x>
- U.T. Probst, Methods for boron analysis in boron neutron capture therapy (BNCT): a review. *Fresenius J. Anal. Chem.* **364**, 391–403 (1999). <https://doi.org/10.1007/s002160051356>
- F.J. Wheeler, D.W. Nigg, J. Capala et al., Boron neutron capture therapy (BNCT): implications of neutron beam and boron compound characteristics. *Med. Phys.* **26**(7), 1237–1244 (1999). <https://doi.org/10.1118/1.598618>
- K. Nedunchezian, N. Aswath, M. Thiruppathy et al., Boron neutron capture therapy—a literature review. *JCDR.* **10**(12), ZE01-ZE04 (2016). <https://doi.org/10.7860/JCDR/2016/19890.9024>
- S. AltieriN, N. Protti, A brief review on reactor-based neutron sources for boron neutron capture therapy. *Ther. Radiol. Oncol.* **2**, 47 (2018). <https://doi.org/10.21037/tro.2018.10.08>
- Y. Sakurai, H. Tanaka, T. Takata et al., Advances in boron neutron capture therapy (BNCT) at kyoto university—from reactor-based BNCT to accelerator-based BNCT. *JKPS.* **67**(1), 76–81 (2015). <https://doi.org/10.3938/jkps.67.76>
- E. Bavarnegin, Y. Kasesaz, F.M. Wagner, Neutron beams implemented at nuclear research reactors for BNCT. *J. Instrum.* **12**, P05005 (2017). <https://doi.org/10.1088/1748-0221/12/05/P05005>
- H. Tanaka, Y. Sakurai, M. Suzuki et al., Improvement of dose distribution in phantom by using epithermal neutron source based on the Be(p, n) reaction using a 30 MeV proton cyclotron accelerator. *Appl. Radiat. Isot.* **67**, S258–S261 (2009). <https://doi.org/10.1016/j.apradiso.2009.03.096>
- N. Hu, H. Tanaka, K. Ono, Design of a filtration system to improve the dose distribution of an accelerator-based neutron capture therapy system. *Med. Phys.* **49**(10), 6609–6621 (2022). <https://doi.org/10.1002/mp.15864>
- H. Tanaka, Y. Sakurai, M. Suzuki et al., Experimental verification of beam characteristics for cyclotron-based epithermal neutron source (C-BENS). *Appl. Radiat. Isot.* **69**(12), 1642–1645 (2011). <https://doi.org/10.1016/j.apradiso.2011.03.020>
- P. Torres-Sánchez, I. Porras, F.A. Saavedra et al., Study of the upper energy limit of useful epithermal neutrons for boron neutron capture therapy in different tissues. *Radiat. Phys. Chem.* **185**, 109490 (2021). <https://doi.org/10.1016/j.radphyschem.2021.109490>
- P. Torres-Sánchez, I. Porras, F.A. Saavedra et al., On the upper limit for the energy of epithermal neutrons for boron neutron capture therapy. *Radiat. Phys. Chem.* **156**, 240–244 (2019). <https://doi.org/10.1016/j.radphyschem.2018.11.015>
- P. Torres-Sánchez, I. Porras, N. Ramos-Chernenko et al., Optimized beam shaping assembly for a 2.1-MeV proton-accelerator-based neutron source for boron neutron capture therapy. *Sci. Rep.* **11**, 7576 (2021). <https://doi.org/10.1038/s41598-021-87305-9>
- E. Bisceglie, P. Colangelo, N. Colonna et al., On the optimal energy of epithermal neutron beams for BNCT. *Phys. Med. Biol.* **45**, 49 (2000). <https://doi.org/10.1088/0031-9155/45/1/304>
- M. Hervé, N. Sauzet, D. Santos., On the epithermal neutron energy limit for accelerator-based boron neutron capture therapy (AB-BNCT): study and impact of new energy limits. *Phys. Med.* **88**, 148–157 (2021). <https://doi.org/10.1016/j.ejmp.2021.06.016>
- R. Seki, Y. Wakisaka, N. Morimoto et al., Physics of epithermal boron neutron capture therapy. *Radiol. Phys. Technol.* **10**(4), 387–408 (2017). <https://doi.org/10.1007/s12194-017-0430-5>
- R.F. Barth, P. Mi, W. Yang, Boron delivery agents for neutron capture therapy of cancer. *Cancer Commun.* **38**(1), 1–15 (2018). <https://doi.org/10.1186/s40880-018-0299-7>
- G. Ichikawa, Development of thermal neutron moderator for testing boron agents for boron neutron capture therapy (BNCT). *J. Instrum.* **14**, T06010 (2019). <https://doi.org/10.1088/1748-0221/14/06/T06010>
- Y. Sakurai, T. Kobayashi, Spectrum evaluation at the filter-modified neutron irradiation field for neutron capture therapy in Kyoto University Research Reactor. *Nucl. Instrum. Methods Phys. Res. A.* **531**(3), 585–595 (2004). <https://doi.org/10.1016/j.nima.2004.05.084>
- G. Ke, Z. Sun, F. Shen et al., The study of physics and thermal characteristics for in-hospital neutron irradiator (IHNI). *Appl. Radiat. Isot.* **67**, S234–S237 (2009). <https://doi.org/10.1016/j.apradiso.2009.03.117>
- K. Watanabe, S. Yoshihashi, A. Ishikawa et al., First experimental verification of the neutron field of Nagoya University Accelerator-driven neutron source for boron neutron capture therapy. *Appl. Radiat. Isot.* **168**, 109553 (2021). <https://doi.org/10.1016/j.apradiso.2020.109553>
- H. Kumada, A. Matsumura, H. Sakurai et al., Project for the development of the linac based NCT facility in University of Tsukuba. *Appl. Radiat. Isot.* **88**, 211–215 (2014). <https://doi.org/10.1016/j.apradiso.2014.02.018>
- L. Porra, T. Seppälä, L. Wendland et al., Accelerator-based boron neutron capture therapy facility at the Helsinki University Hospital. *Acta Oncol (Madr)*. **61**(2), 269–273 (2022). <https://doi.org/10.1080/0284186X.2021.1979646>

30. J. Chen, Z. Hu, J. Tong et al., Study of BNCT neutronics optimization for out-of-beam dosimetry based on radiobiological figures of merit. *Nucl. Instrum. Methods Phys. Res. B* **508**, 1–9 (2021). <https://doi.org/10.1016/j.nimb.2021.09.014>
31. R. Edgecock, Accelerator-driven boron neutron capture therapy. *Int. J. Mod. Phys. A* **29**, 1441004 (2014). <https://doi.org/10.1142/S0217751X14410048>
32. C. Ceballos, J. Esposito, S. Agosteo et al., Towards the final BSA modeling for the accelerator-driven BNCT facility at INFN LNL. *Appl. Radiat. Isot.* **69**(12), 1660–1663 (2011). <https://doi.org/10.1016/j.apradiso.2011.01.032>
33. K. Tsujimoto, Accelerator-based neutron source and its application. In: *Plasma Conference 2011 (PLASMA 2011)*. Kannazawa(Janpan), pp. 1–2 (2011)
34. Y. Kiyonagi, Accelerator-based neutron source for boron neutron capture therapy. *Ther. Radiol. Oncol.* **2**, 55 (2018). <https://doi.org/10.21037/tro.2018.10.05>
35. M.S. Herrera, S.J. González, D.M. Minsky et al., Evaluation of performance of an accelerator-based BNCT facility for the treatment of different tumor targets. *Phys. Med.* **29**(5), 436–446 (2013). <https://doi.org/10.1016/j.ejmp.2013.01.006>
36. N. Hu, H. Tanaka, S. Yoshikawa et al., Development of a dose distribution shifter to fit inside the collimator of a Boron Neutron Capture Therapy irradiation system to treat superficial tumours. *Phys. Med.* **82**, 17–24 (2021). <https://doi.org/10.1016/j.ejmp.2021.01.003>
37. A. Sasaki, N. Hu, T. Takata et al., Intensity-modulated irradiation for superficial tumors by overlapping irradiation fields using intensity modulators in accelerator-based BNCT. *J. Radiat. Res.* **63**(6), 866–873 (2022). <https://doi.org/10.1093/jrr/trac052>
38. Z. Qiao, B. Ma, B. Rong et al., Beam shaping assembly design of Li(p, n) neutron source with a rotating target for boron neutron capture therapy. *Nucl. Instrum. Methods Phys. Res. A* **1052**, 168249 (2023). <https://doi.org/10.1016/j.nima.2023.168249>
39. I. Murata, S. Tamaki, S. Kusaka et al., Neutronics design of fusion reactor-based boron neutron capture therapy in ITER. *Fusion Sci. Technol.* **79**, 465–475 (2023). <https://doi.org/10.1080/15361055.2022.2151280>
40. Y. Hashimoto, F. Hiraga, Y. Kiyonagi, Optimal moderator materials at various proton energies considering photon dose rate after irradiation for an accelerator-driven ${}^9\text{Be}(p, n)$ boron neutron capture therapy neutron source. *Appl. Radiat. Isot.* **106**, 88–91 (2015). <https://doi.org/10.1016/j.apradiso.2015.07.027>
41. R. Inoue, F. Hiraga, Y. Kiyonagi, Optimum design of a moderator system based on dose calculation for an accelerator driven boron neutron capture therapy. *Appl. Radiat. Isot.* **88**, 225–228 (2014). <https://doi.org/10.1016/j.apradiso.2013.12.017>
42. Z. Guo, C. Liu, W. Zhang et al., Optimization design of BNCT neutron source and moderating body based on accelerator ${}^7\text{Li}(p, n)$ reaction. *Nuclear Techniques (in Chinese)* **45**, 050201 (2022). <https://doi.org/10.11889/j.0253-3219.2022.hjs.45.050201>
43. Y. Lu, W. Li, Z. Xu et al., Experimental terminal design of BNCT neutron source based on 14 MeV proton cyclotron. *Nuclear Techniques (in Chinese)* **45**, 030202 (2022). <https://doi.org/10.11889/j.0253-3219.2022.hjs.45.030202>
44. Y. Zhu, Z. Lin, L. Lu et al., Design of beam shaping assembly for boron neutron capture therapy based on D-T neutron source. *Nuclear Techniques (in Chinese)* **45**, 010202 (2022). <https://doi.org/10.11889/j.0253-3219.2022.hjs.45.010202>
45. C.J. Malmer, ICRU Report 63. Nuclear data for neutron and proton radiotherapy and for radiation protection. *Med. Phys.* **28**(5), 861 (2001). <https://doi.org/10.1118/1.1369116>
46. F. Naito, Introduction to accelerators for boron neutron capture therapy. *Ther. Radiol. Oncol.* **2**, 54 (2018). <https://doi.org/10.21037/tro.2018.10.11>
47. S. Masunaga, Y. Sakurai, H. Tanaka et al., The dependency of compound biological effectiveness factors on the type and the concentration of administered neutron capture agents in boron neutron capture therapy. *Springerplus* **3**(1), 128 (2014). <https://doi.org/10.1186/2193-1801-3-128>
48. JANIS Books. (2023). <https://www.oecd-nea.org/janisweb/book/neutrons/H1/MT2/render/735>

Springer Nature or its licensor (e.g. a society or other partner) holds exclusive rights to this article under a publishing agreement with the author(s) or other rightsholder(s); author self-archiving of the accepted manuscript version of this article is solely governed by the terms of such publishing agreement and applicable law.